CrystEngComm

ROYAL SOCIETY OF CHEMISTRY

HIGHLIGHT

Cite this: *CrystEngComm*, 2022, **24**, 2189

Metal–organic frameworks with ftw-type connectivity: design, pore structure engineering, and potential applications

Xingyu Li,[ab] Hao Wang, *[a] Jizhao Zou *[b] and Jing Li *[ac]

Received 11th January 2022,
Accepted 10th February 2022

DOI: 10.1039/d2ce00044j

rsc.li/crystengcomm

Metal–organic frameworks (MOFs) feature intrinsically structural diversity and high tunability with respect to porosity and functionality. By practice of reticular chemistry, the pore size, pore shape, and pore surface chemistry of MOFs can be systematically and precisely tuned. MOFs with **ftw** topology represent an extensively studied family for which reticular chemistry has been well implemented. In this article, advances in the development of **ftw**-type MOFs and their related applications are reviewed. In particular, we focus on the tuning of pore size and pore shape by ligand design as well as SBU modification for targeted applications. In addition, the existing challenges and possible future directions of this important research field will be briefly discussed.

1. Introduction

Metal–organic frameworks (MOFs) are a remarkable family of porous materials having intrinsic tunability in their crystal structure, porosity, pore shape and dimensions, and pore surface functionality as a result of nearly unlimited combinations of their inorganic nodes and organic linkers. The formulation and implementation of reticular chemistry, pioneered by Yaghi and co-workers, has largely facilitated the development of MOFs with precisely tailored structure and properties.[1] Reticular chemistry allows one to finely tune the porosity, pore shape, size, and surface chemistry of a MOF without altering its overall connectivity. Representative practice of reticular chemistry includes pore augmentation and/or surface functionalization of IRMOFs (**pcu**),[2] the MOF-74 series (**etb**),[3] and the UiO family (**fcu**).[4]

The rapid development of MOFs based on early transition metals, for example Zr-MOFs, over the past decade has further facilitated the wide implementation of reticular chemistry.[5] Zr-MOFs are predominately built on hexanuclear Zr_6 SBUs, thus the connectivity and topology of Zr-MOFs are largely dictated by the geometry and dimensions of organic linkers. For example, linear dicarboxylates usually form **fcu** topology with Zr while square/rectangular-shaped tetracarboxylates typically form **ftw** or its derivative topology

[a] *Hoffmann Institute of Advanced Materials, Shenzhen Polytechnic, 7098 Liuxian Boulevard, Shenzhen, Guangdong 518055, P. R. China. E-mail: wanghao@szpt.edu.cn*
[b] *College of Materials Science and Engineering, Shenzhen University, Shenzhen, 518060, PR China. E-mail: zoujizhao@szu.edu.cn*
[c] *Department of Chemistry and Chemical Biology, Rutgers University, 123 Bevier Road, Piscataway, New Jersey 08854, USA. E-mail: jingli@rutgers.edu*

Xingyu Li

Xingyu Li obtained his B.S. degree from North University of China in 2018. He is currently a graduate student at the Shenzhen University under the supervision of Prof. Jizhao Zou with a collaborative program with Hoffmann Institute of Advanced Materials (HIAM) at Shenzhen Polytechnic, under the guidance of Prof. Hao Wang. His research focuses on the design, synthesis, and application of stable MOFs.

Hao Wang

Hao Wang received his B.S. degree from Wuhan University, China, in 2012, and Ph.D. degree from Rutgers University, United States, in 2018. He then joined the Hoffmann Institute of Advanced Materials (HIAM) at Shenzhen Polytechnic, where he is currently an associate professor. His research focuses on the design of novel crystalline porous materials and their applications in adsorption and separation.

(such as **scu**, **lvt**, *etc.*) with Zr.[5,6] By changing the length and functional groups of linear dicarboxylate linkers, more than a hundred of Zr-MOFs with **fcu** topology have been achieved.[6] These materials feature exceptional stability, high porosity (BET surface area typically 300–4000 $m^2\ g^{-1}$), a wide range of pore apertures (~5–20 Å), and diverse surface chemistry. They are targeted for various applications, including adsorption/capture,[7,8] catalysis,[9,10] and drug delivery,[11] to name a few.

Similar to **fcu**-MOFs, MOFs featuring **ftw** topology are also commonly built on 12-connected hexanuclear SBUs, but with planar, tetratopic linkers instead of linear dicarboxylates. The hexanuclear SBUs are not limited to Zr_6, Hf_6, and Y_6,[12,13] but also include late transition metals such as Ni_6.[14–16] Besides planar tetracarboxylates, tetra-pyrazolates and the 4-connected coordination complex can also serve as the organic linkers in **ftw** structures.[17] In this highlight article, we provide an overview of the research progress on **ftw**-type MOFs, from regulating their structure, pore size and surface chemistry to assessing their potential applications, with an emphasis on the implementation of reticular chemistry for the development of these MOFs with precisely tailored pore structure and functionality.

2. Structure of ftw-MOFs

MOFs with **ftw** topology feature a (4,12)-connected edge transitive binodal net built on 12-connected cuboctahedral vertexes and 4-connected square or rectangle faces (Fig. 1). The 12-c vertexes are generally hexanuclear M_6N_x (M = Zr^{4+}, Hf^{4+}, Y^{3+}, Tb^{3+} *etc.*, N = O^{2-}, OH^-, F^-, *etc.*) clusters. For an ideal **ftw** structure, the 4-c strut should be a square. However, a rectangular linker (aspect ratio larger than 1) could also fit into an **ftw** structure by alternating the orientation of the rectangle as well as rotating the 12-c vertex, which has been observed in a series of **ftw**-MOFs (Scheme 1).[13]

In general, **ftw**-MOFs possess highly stable frameworks as a result of the robust hexanuclear SBUs with high connectivity, as well as the M–O bonds incorporating M^{4+} or M^{3+} with high valence. The **ftw** topology is recognized to have the highest porosity and lowest propensity for framework catenation, making it desirable for adsorption related applications.[18] Particularly, **ftw**-MOFs feature cage-like pores with large cavities interconnected by small windows which is ideal for molecular separation as the large cavities can guarantee high adsorption capacity while the small windows serve as gates for splitting or discriminating different adsorbates (Table 1).

3. ftw-MOFs built on large organic linkers

Porphyrinic linkers

In 2012, Yaghi *et al.* reported two **ftw**-MOFs by combining 12-c Zr_6 clusters and square porphyrinic tetracarboxylates: MOF-525 ($Zr_6O_4(OH)_4(TCPP\text{-}H_2)_3$) and MOF-535 ($Zr_6O_4(OH)_4(XF)_3$).[20] In their structures, 12-connected hexanuclear SBUs $Zr_6O_4(OH)_4(COO)_{12}$ serve as vertexes of the **ftw** net, which are interconnected by 4-connected tetratopic organic linkers occupying the centers of the faces (Fig. 2). In MOF-525, the organic linker $[TCPP\text{-}H_2]^{4-}$ is square-shaped and thus fits perfectly in the resultant ideal **ftw** net. Its 12-connected Zr_6 cluster binds 12 carboxylates from 12 different organic linkers. This is different from the porphyrinic Zr-MOFs PCN-222 and PCN-224 reported at a later time for which the connection number of the Zr_6 cluster is reduced to 8 and 6, respectively. In contrast, in the structure of MOF-535, XF^{4-} is not an ideal square, however, it displays a conformational flexibility that allows the formation of the final **ftw** network. Both MOF-525 and MOF-535 exhibit exceptional chemical stability and high porosity. These compounds are stable in methanol, water, and acidic solutions. The Brunauer–Emmett–Teller (BET) surface areas of MOF-525 and MOF-535 are 2620 and 1120 $m^2\ g^{-1}$, respectively.

Extensive studies have been carried out on **ftw**-MOFs built on hexanuclear Zr_6 clusters and porphyrin-derived tetracarboxylates linkers since the report of MOF-525. Almost simultaneously in 2015, a series of new porphyrinic **ftw**-Zr-MOFs were developed independently by several different

Jizhao Zou

Jizhao Zou received his doctor's degree in Northwestern Polytechnical University in 2007. He then joined Shenzhen University as Assistant Professor and was promoted to Associate Professor in 2012. His current research mainly focuses on the preparation of porous carbon materials and their applications in energy-related field.

Jing Li

Jing Li received her Ph.D. degree from Cornell University in 1990 under the guidance of Professor Roald Hoffmann. She joined the chemistry faculty at Rutgers University in 1991 as Assistant Professor. She was promoted to Associate Professor in 1996, to Full Professor in 1999, and to Distinguished Professor in 2006. Her research focuses on designing and developing new and functional materials (including MOFs and hybrid semiconductors) for renewable, sustainable and clean energy related applications.

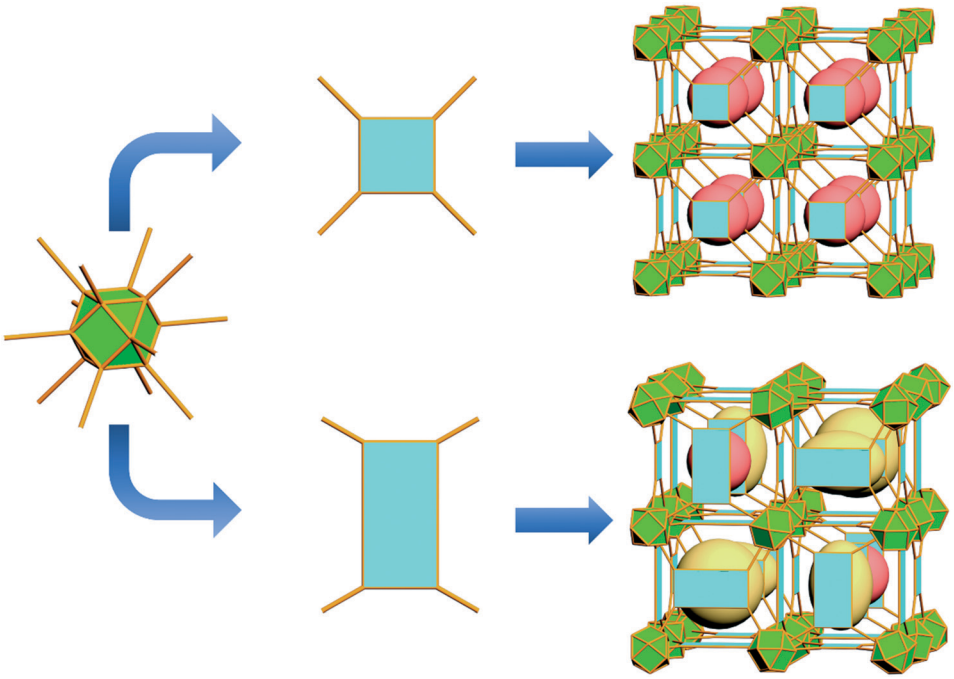

Fig. 1 Schematic of **ftw**-MOFs built on square or rectangle shaped organic linkers.

research groups of Zhou, Feng, Su, Farha and their coworkers. Zhou *et al.* reported the topology-guided design and synthesis of a series of three **ftw**-Zr-MOFs, PCN-228, PCN-229, and PCN-230, built on elongated $TCPP^{4-}$ (tetracarboxyphenylporphyrin) linkers.[23] It is worth mentioning that the molecular structures of the three organic linkers, H_4TCP-1, H_4TCP-2, and H_4TCP-3, were deliberately tailored with desired confirmation by carefully arranging the vicinal phenyl rings and carboxylate groups so that they would fit into **ftw**-type frameworks. The three compounds are isoreticular to MOF-525 and network interpenetration, which has been commonly observed in isoreticular expansion of MOFs, was prevented presumably by the bulky porphyrin rings. Ligand elongation successfully expands the pore apertures from micropores in MOF-525 to mesopores in PCN-228-230. The pore apertures of the three compounds are in the range of 2.5 to 3.8 nm and their BET surface areas are in the range of 4450 to 4619 $m^2\ g^{-1}$. The exceptionally high porosity and open network did not alter the stability of the **ftw**-MOFs. Similar to MOF-525, PCN-228-230 featured high chemical stability and its crystallinity and porosity were completely retained upon treatments of aqueous solutions with a wide range of pH from 0 to 12. The authors attributed the excellent chemical stability of these materials to the fully connected Zr_6 clusters. Feng *et al.* reported a series of four isostructural heterometallic zirconium metalloporphyrin frameworks (CPM-99) with different chelating metals.[25] They feature the same structure as that of PCN-228 and the uniformly embedded metallo-porphyrin centers make the compounds promising precursors for oxygen reduction reaction (ORR) catalysts. Farha *et al.* reported two **ftw**-Zr-MOFs with elongated porphyrinic ligands (Por-PP and Por-PTP).[24] The molecular structure of Por-PP and Por-PTP are similar to H_4TCP-1 and H_4TCP-2, respectively, but the former are not functionalized with alkyl groups. The resulting MOFs, NU-1102 and NU-1104, feature expected **ftw** topology. NU-1102 and NU-1104 displayed exceptionally high BET surface areas of 4830 and 6230 $m^2\ g^{-1}$, respectively. These values are higher than that of the TCP-based series, which could be attributed to their less bulkier organic linkers as well as possibly more complete activation. Wu *et al.* reported the **ftw**-type Zr and Hf MOF built on H_2TBPP^{2-} (Por-PP): FJI-H6 (Zr) and FJI-H7 (Hf). The Zr and Hf analogues are isostructural to that of NU-1102.[12]

More recently, Deng *et al.* reported a series of mesoporous **ftw**-Zr-MOFs (MOF-526, MOF-527, and MOF-528) built on elongated porphyrinic tetrabenzoates linkers with copper coordinating porphyrin units in the center (TCBPP-Cu, TCTPP-Cu, and TCTTPP-Cu).[32] MOF-526–528 exhibit high porosity with BET surface areas of 4260, 2000, 3550 $m^2\ g^{-1}$, respectively, and excellent chemical stability. The authors investigated the reversible π-interactions between the mesoporous MOFs and various large organic guest molecules in aqueous solutions. It was revealed that the π-interaction sites were capable of repetitive and reversible dynamics in interacting with large polycyclic hydrocarbons in water, where each site attracted two guest molecules in a quantitative manner.

Pyrene-based linkers

Besides porphyrinic ligands, pyrene-derived carboxylates have also been commonly used for the construction of **ftw**-MOFs as a result of their square-shaped core. Farha *et al.* reported an **ftw**-Zr-MOF, NU-1100, built on pyrene-based tetra-ethynyl-

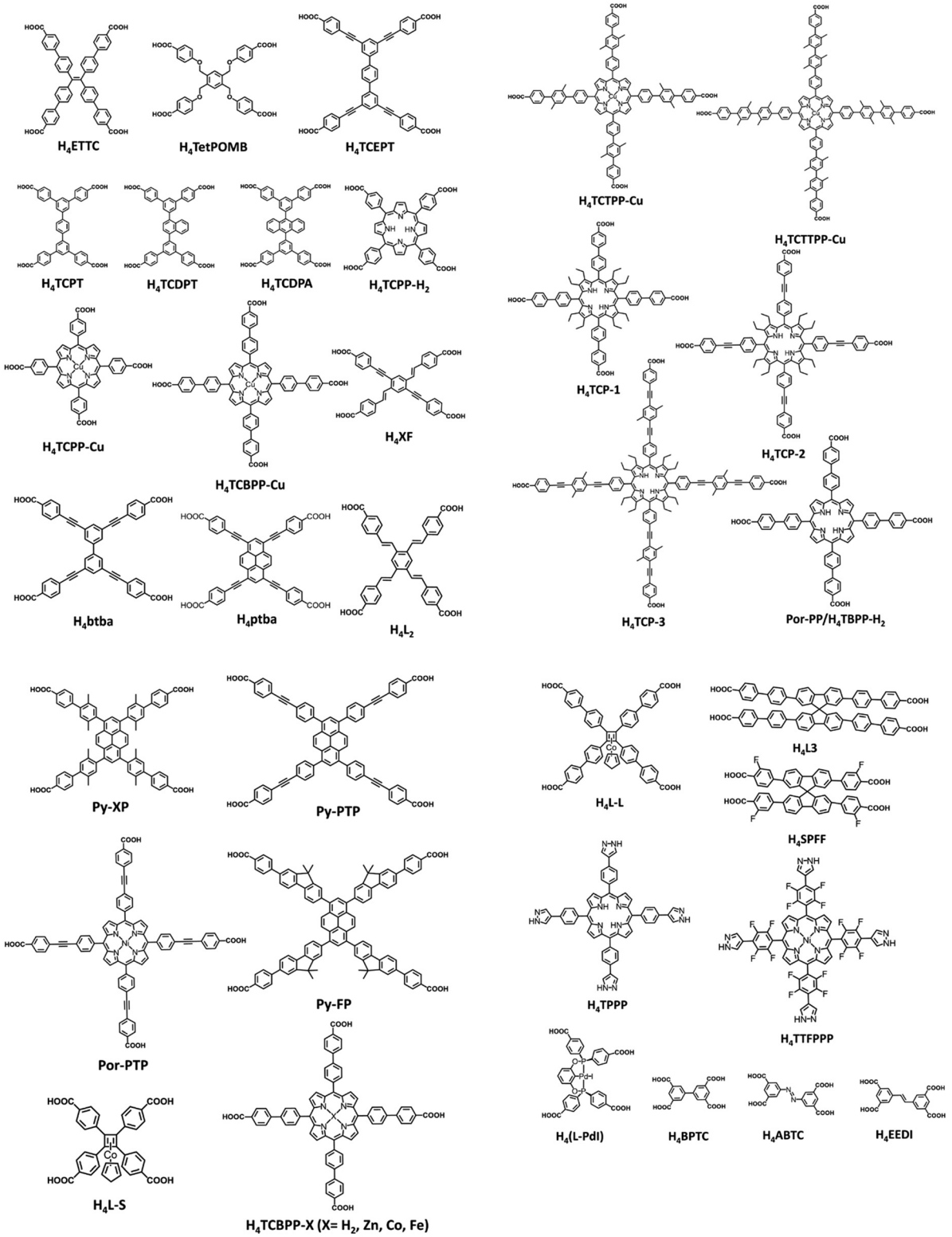

Scheme 1 Representative organic linkers used for the construction of **ftw**-MOFs.

benzoates.[22] NU-1100 represented the first example of isoreticular expansion of **ftw**-Zr-MOFs after MOF-525 and MOF-535. It is interesting that the orientation of the organic linkers is different in adjacent nearly-cubic boxes, with two possible combinations of the box faces that finally form a supercube (Fig. 3). This should be attributed to the fact that the ligand is a rectangle rather than a square. The MOF features exceptional porosity with a BET surface area of 4020

Table 1 Representative reported **ftw**-MOFs

MOF	Metal	Ligand (aspect ratio)	BET surface area ($m^2\ g^{-1}$)	Cage size (window size) (Å)	Year of report	Ref.
$Co_9(btc)_6(tpt)_2$	Co	—	—	—	2011	19
MOF-525	Zr	$H_4TCPP\text{-}H_2$ (1.0)	2620	20	2012	20
MOF-535	Zr	H_4-XF (1.0)	1120	—	2012	20
PCN-94	Zr	ETTC (1.0)	3377	17.5(14)	2014	21
NU-1100	Zr	H_4L_1 (1.03)	4020	—	2014	22
PCN-228	Zr	H_4TCP-1 (1.0)	4510	25	2015	23
PCN-229	Zr	H_4TCP-2 (1.0)	4619	28	2015	23
PCN-230	Zr	H_4TCP-3 (1.0)	4455	38	2015	23
NU-1101	Zr	Py-XP (1.0)	4340	24.3	2015	24
NU-1102	Zr	Por-PP (1.0)	4830	25.3	2015	24
NU-1103	Zr	Py-PTP (1.0)	6550	27.9	2015	24
NU-1104	Zr	Por-PTP (1.0)	6230	28.9	2015	24
CPM-99	Zr	TCBPP-X (1.0)	1030	25	2015	25
FJI-H6	Zr	$H_4TBPP\text{-}H_2$ (1.0)	5033	25(20)	2015	12
FJI-H7	Hf	$H_4TBPP\text{-}H_2$ (1.0)	3831	25(20)	2015	12
NU-1105	Zr	Py-FP (1.0)	3700	—	2015	26
—	Zr	H_4(btba) (1.0)	4342	18.7(7.6)	2015	27
—	Zr	H_4(ptba) (1.0)	4116	18	2015	27
Y-**ftw**-MOF-1	Y	TetPOMB (1.0)	—	19	2015	13
Y-**ftw**-MOF-2	Y	TCPT (1.29)	3690	21	2015	13
Y-**ftw**-MOF-3	Y	TCEPT (1.12)	—	23	2015	13
Y-**ftw**-MOF-2 (Naphth)	Y	TCDPN (—)	3040	14	2015	13
Y-**ftw**-MOF-2 (Anth)	Y	TCDPA (—)	2100	14	2015	13
PCN-601	Ni	H_4TPP (—)	—	—	2016	16
—	Zr	H_4(L-PdI) (1.15)	1164	—	2016	28
PCN-602	Ni	H_4TPPP (1.0)	2219	—	2017	15
ftw-MOF-BPTC/Y-bptc	Y	H_4BPTC (1.45)	319	9.5(3.0)	2018	29, 30
ftw-MOF-ABTC	Tb	H_4ABTC (1.81)	—	9.6(4.4)	2018	30
Zr-bptc	Zr	H_4BPTC (1.45)	1318	12(4.5)	2018	18
Y-abtc	Y	H_4ABTC (1.83)	427	—	2018	29
MOF-1	Zr	H_4L_2 (—)	896	19	2018	31
MOF-1211	Zr	$H_4CoCl_2(NC_5H_4CO_2)_4$	925	—	2018	17
PCN-624	Ni	$H_4TTFPPP$ (1.0)	2010	—	2018	14
MOF-526	Zr	$H_4TCBPP\text{-}Cu$ (1.0)	4260	25.5(12)	2019	32
MOF-527	Zr	$H_4TCTPP\text{-}Cu$ (1.0)	2000	31.4	2019	32
MOF-528	Zr	$H_4TCTTPP\text{-}Cu$ (1.0)	3550	37.6(21)	2019	32
MOF-536	Zr	$H_4TCPP\text{-}Fe$ (1.0)	2010		2019	32
Eu-SPFF	Eu	H_4SPFF (—)	1891	19.5(8.5)	2019	33
Zr-IAM-4	Zr	H_4L_3 (1.0)	1685	25.2	2020	34
RhCu-**ftw**-MOF-1	Rh/Cu	$HINA/H_3BTC$	400	—	2021	35
UPC-612	Zr	H_4L-L (—)	2016	20	2021	36
UPC-613	Zr	H_4L-S (—)	853	15.7	2021	36
HIAM-301	Y	H_4eedi (—)	579	10(4.6)	2021	37

Notes: —: not reported.

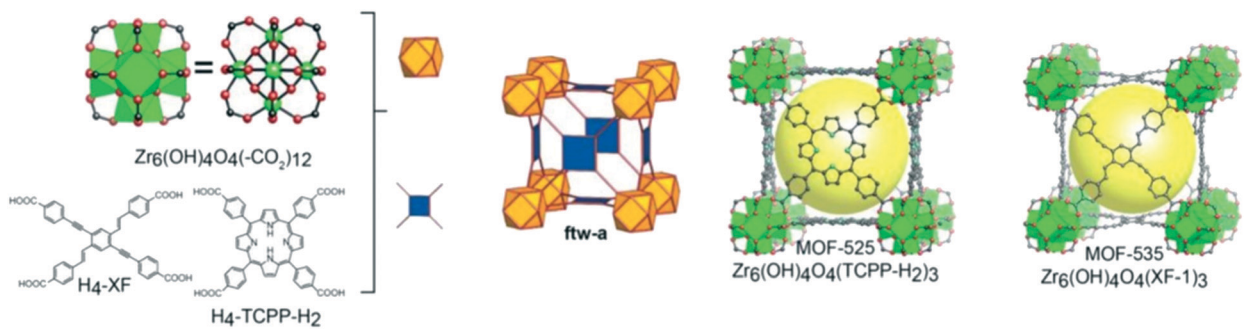

Fig. 2 Crystal structures of MOF-525, and –535. Reproduced with permission.[20] Copyright 2012, American Chemical Society.

$m^2\ g^{-1}$ and a pore volume of 1.53 $cm^3\ g^{-1}$. NU-1100 is highly robust in water and fully retains its crystallinity and porosity after soaking in water. It takes up 43 g L^{-1} hydrogen at 65 bar and 77 K, and 180 V_{STP}/V methane at 65 bar and 298 K. Later the same research group used two further elongated pyrene-derived organic linkers, Py-XP (NU-1101) and Py-PTP (NU-

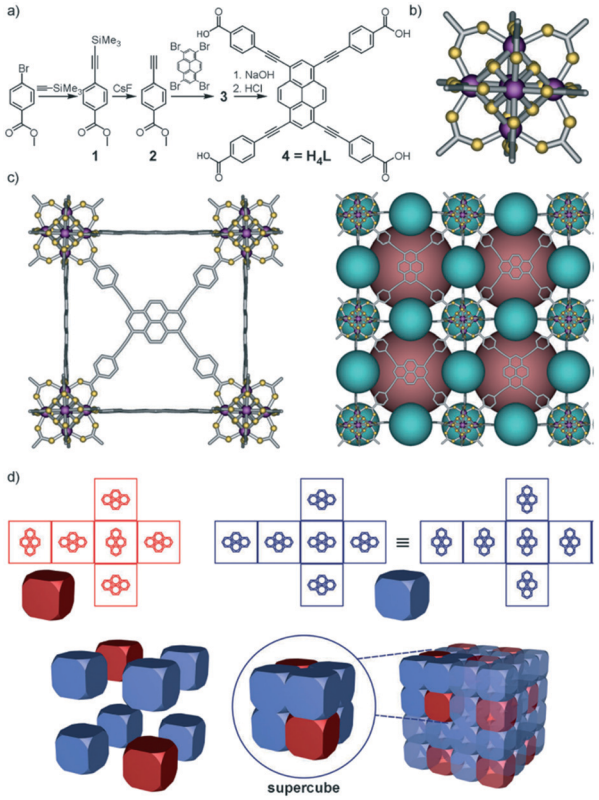

Fig. 3 a) Scheme for H_4L synthesis. b) and c) Structural elements and crystal packing of NU-1100 (Zr atoms are shown as purple spheres, O atoms as yellow spheres, and the carbon skeleton as gray sticks). Dark pink and light blue spheres occupy two major pore types in the crystal. d) Schematic representation of NU-1100 supramolecular structure as a superposition of two different cubes (red and blue). Reproduced with permission.[22] Copyright 2014, Wiley-VCH.

1103), to form two **ftw**-Zr-MOFs with even higher porosity.[24] It is noteworthy that for **ftw**-MOFs built on large organic linkers, such as NU-1101 and NU-1103 or the previously mentioned NU-1100, there are two kinds of pores in the structure: large pores located at the center of the cubic box and small pores located at the edges of the cubic box. This is different from those built on down-sized organic linkers which do not have accessible voids at the edges. NU-1101 and NU-1103 are also stable in water despite their highly open structure. The experimental BET surface areas of NU-1101 and NU-1103 are 4340 and 6550 $m^2\ g^{-1}$, respectively. The latter represents the most porous **ftw**-MOF reported so far. It is worthwhile to mention that, with a pair of pore types with different dimensions, nitrogen adsorption isotherms of these MOFs showed a sharp and sizable step at P/P_0 values between 0.1 and 0.2. This caused the BET theory to overestimate the monolayer coverage as well as the surface area values. The authors therefore suggested to pay attention to the discrepancy between the measured BET surface area and the geometric surface area.

In a separate study, Farha *et al.* reported an ultraporous and breathing **ftw**-Zr-MOF, NU-1105, built on fluorine-benzoate functionalized pyrene-derived organic linker (Py-FP).[26] It is interesting that the compound undergoes a structure breathing between NU-1105-op and NU-1105-cp upon guest removal and inclusion, which has been rarely observed for **ftw**-MOFs. Further insights into the structural transformation by computational modeling revealed that the structure flexibility originates from the bent long arm of the Py-FP linker. The structural breathing behavior was also reflected by a notable hysteresis in its adsorption–desorption isotherm of propane. The measured BET surface area and pore volume of NU-1105-cp from nitrogen adsorption at 77 K were 3700 $m^2\ g^{-1}$ and 2.17 cc g^{-1}, respectively. The pore volume is 26% lower than the GCMC-simulated value for NU-1105-op, and this is consistent with the pore volume reduction expected from the X-ray derived lattice constants. This study suggested that by incorporating flexible, long organic linkers with the Zr–oxo nodes, it is possible to develop ultraporous, water-stable, breathing MOFs. These types of materials may be potentially useful for gas or vapor storage with high working capacities.

Two **ftw**-Zr-MOFs were realized by Rosseinsky *et al.* through linker engineering.[27] Two similar tetrabenzoate linkers with the same four-fold connectivity were used to construct **ftw**-MOFs. However, the two linkers differ in flexibility: the pyrene-based H_4ptba is rigidly planar, whereas the biphenyl-based H_4-btba has one extra torsional degree of freedom. As expected, two **ftw**-MOFs were achieved by the combination of Zr–oxo nodes and each individual linker. Pronounced deviations from planarity in the ligand conformation were observed for Zr-btba which is expected considering its flexibility. In the structure of Zr-ptba, about 8% of the ptba linkers were missing, which is not uncommon for Zr-MOFs.[38] However, neither of the two MOFs is as robust as the previously reported **ftw**-Zr-MOFs. Significant care was required in activating Zr-btba to attain the anticipated porosity, whereas Zr-ptba lost its crystallinity and porosity upon water treatment. The authors attributed the lack of structural stability of Zr-btba and Zr-ptba to the flexible linker leading to the deviation from planarity and linker deficiency, respectively. To address the issue, the authors incorporated both linkers into one MOF structure. Three analogous **ftw**-MOFs with different mixed-linker ratios and different degrees of linker defects were achieved. In particular, the analytically pure multiple linker-based compound showed high porosity with simple activation. In addition, the highly robust framework remained intact in water. The results suggested that the multilinker approach may be effective to produce highly porous MOFs with enhanced properties arising from synergy between linker chemistries.

TPE-based linkers

Tetraphenylethylene (TPE) derived organic ligands have been extensively studied for the construction of MOFs in light of its aggregation-induced emission (AIE) character. In particular, $ETTC^{4-}$, with a tetrabenzoate functionalized TPE core, was incorporated into an **ftw**-Zr-MOF PCN-94 by Zhou *et al.*[21] The organic linker H_4ETTC emits yellow light at 545 nm with a

quantum yield of 30.0% (Fig. 4). Interestingly, by rigidifying it into the MOF structure, a notable blue shift of fluorescence and enhancement of quantum yield were observed. PCN-94 emits blue light at 470 nm with quantum yields of 76.2% and 99.9% in air and Ar, respectively. The substantial increase in quantum yield from the free organic linker to the MOF compound was attributed to the reduced intra- and intermolecular interactions by rigidifying the linker.

Spiro-based linkers

Spiro-derived tetrabenzoate molecules feature rigid, planar characters which are suitable for the formation of **ftw**-MOFs. Li *et al.* reported an **ftw**-MOF built on hexanuclear Eu_6 clusters and a fluoro-functionalized, spiro-derived organic ligand ($SPFF^{4-}$).[33] The four carboxylate groups of the $SPFF^{4-}$ ligand in the MOF structure lie roughly in the same plane and thus the ligand is close to a square that fits well into the **ftw** topology.

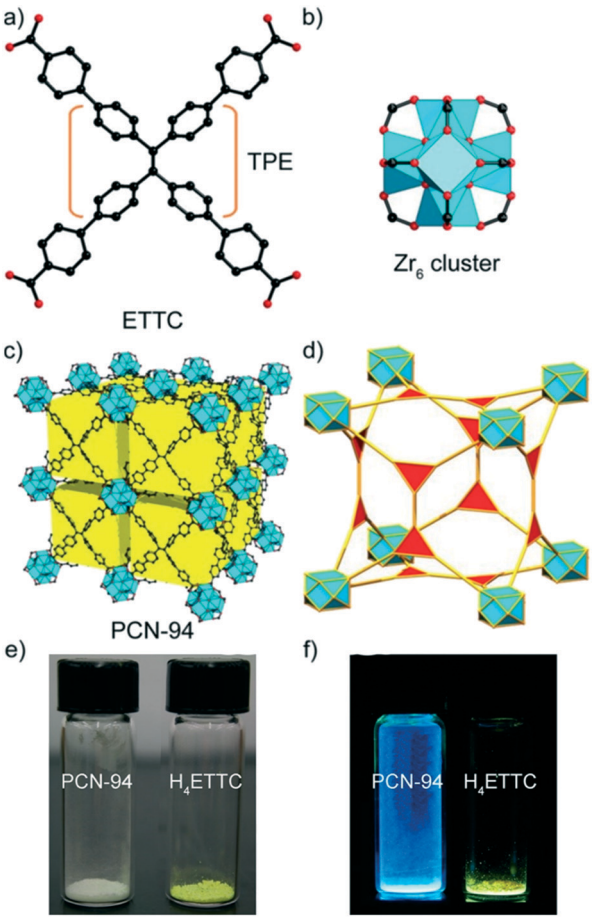

Fig. 4 (a–d) Crystal structure views of PCN-94 showing: (a) ETTC in PCN-94; orange brackets indicate the TPE core; (b) Zr6 cluster; (c) PCN-94 framework; (d) topological representation of PCN-94. All H atoms are omitted, and only one orientation of the disordered atoms is shown for clarity. Color scheme: black, C; red, O; blue polyhedron, Zr; yellow cube, cavity with 17.5 Å edge. Photos of PCN-94 and H_4ETTC are shown under (e) ambient light and (f) UV light. Reproduced with permission.[21] Copyright 2014, American Chemical Society.

Eu-SPFF has a BET surface area of 1891 $m^2\ g^{-1}$ and a pore volume of 0.79 $cm^3\ g^{-1}$. The MOF was further studied for the separation of light hydrocarbons as well as fluorescence recognition of explosives and heavy metals. More recently, Zhao *et al.* reported a family of isostructural **ftw**-MOFs constructed from a spirobifluorene-center tetracarboxylate linker and hexanuclear clusters built on various metals including Zr or Ln (Ln = Eu, Tb, Gd, Dy, Tm, Yb, Nd, and Er).[34] Interestingly, they all feature doubly interpenetrated framework which is rarely observed for **ftw**-MOFs. This unique structural feature was attributed to the specific geometry of the spirobifluorene-linker. In the previously discussed **ftw**-MOFs, each face of the cubic cage is occupied by bulky tetracarboxylate linkers with highly conjugated π-systems such as porphyrin or pyrene rings in the center leaving limited space for an additional linker which inherently prevents the occurrence of interpenetration. In contrast, the two orthogonally connected fluorine rings of the spirobifluorene-linker are perpendicular to the face of the cubic cage leading to a window that is large enough to accommodate the other independent net. This work provides some insights on developing robust, interpenetrated **ftw**-MOFs.

Other linkers

Besides the aforementioned groups of linkers, other organic ligands with planar, square or rectangle shaped tetratopic ligands have also been used for building **ftw**-MOFs. Eddaoudi *et al.* reported a series of **ftw**-MOFs combining rare earth metal based hexanuclear clusters and a variety of square (TetPOMB) or rectangular (TCPT, TCEPT, TCDPN, TCDPA) tetracarboxylate ligands.[13] The authors in this work explored the underlying relations between the structural features of MOFs and the geometry of the organic linkers. The flexibility of TetPOMB permits adoption of the necessary geometry (a square) to allow the formation of a MOF, **ftw**-MOF-1 with Y, Tb, or Yb, with the ideal **ftw** topology. However, the permanent porosity of **ftw**-MOF-1 was not detected by gas adsorption as the attempts to its activation resulted in loss of crystallinity. The lack of structural robustness was attributed to the flexibility of the ligand. For the rectangular ligands, **ftw**-MOFs could be accessed by the rotation of the inorganic hexanuclear SBU, as well as the alternation in the orientation of the ligands. The resulting MOF structures feature a novel (3,3,12)-c net derived from the parent **ftw**-net (kle). Indeed, these **ftw**-MOFs incorporating relatively rigid rectangular ligands exhibit high thermal stability.

Zhao *et al.* reported an **ftw**-Zr-MOF constructed from a square, tetrabenzoate functionalized tetra-vinyl benzene.[31] The MOF is structurally robust and has a BET surface area of 896 $m^2\ g^{-1}$. Very recently, Sun *et al.* reported one-step ethylene purification from an acetylene/ethylene/ethane ternary mixture by **ftw**-Zr-MOFs built on cyclopentadiene cobalt-functionalized ligands.[36] The structures of these MOFs, UPC-612 and UPC-613, are similar to that of MOF-525. The introduction of the cyclopentadiene cobalt functional group led to increased host–guest interaction and efficient separation of ethylene from the hydrocarbon mixtures.

4. ftw-MOFs built on small organic linkers

As mentioned in the previous section, the early examples of **ftw**-MOFs are generally built on large organic ligands with a porphyrin or pyrene core and a square- or rectangular-shape. Their orientation in the MOF structures and their effect on the framework stability, porosity, and related properties have been discussed. However, these delicate ligands involve complicated organic synthesis, and due to their large molecular dimensions, the resulting MOFs may have pore apertures that are too large for adsorptive separation related applications. To address this issue, a series of **ftw**-MOFs constructed from small tetratopic ligands have been developed and explored for adsorption-related applications.

Li *et al.* reported the first example of isoreticular contraction of **ftw**-Zr-MOFs.[18] To downsize the pore aperture of **ftw**-Zr-MOFs and make use of them for molecular separation of industrially relevant hydrocarbons, the authors attempted to develop structures based on isophthalate-based tetracarboxylate linkers, $bptc^{4-}$, $abtc^{4-}$, and $tptc^{4-}$ (Fig. 5). The accessible pore window size of an **ftw**-structure is essentially related to the distance between adjacent carboxylates of the organic ligand. Thus these small-sized tetracarboxylate linkers would potentially result in suitable pore dimensions if they can fit into **ftw**-MOFs. The results indicated that the combination of $bptc^{4-}$ and the hexanuclear Zr_6 cluster led to the formation of the expected **ftw**-type structure, Zr-bptc. The compound featured exceptional thermal and water stability that should be attributed to the fully connected hexanuclear Zr_6 SBU and the rigid organic linker. As a result of the incorporation of the small-sized isophthalate-based ligand, Zr-bptc possesses cage-like pores with a cage size of ~12 Å interconnected by small windows of ~4.5 Å. Thus for the first time the pore aperture of **ftw**-Zr-MOFs was tuned to be within the ultramicroporous region. Zr-bptc behaves like a molecular sieve that fully separates linear and branched alkanes through selectively size-exclusion, but with an adsorption capacity 70% higher than that of zeolite 5A under identical conditions. This preferred behavior can be attributed to its high porosity and suitable pore aperture and the study suggests that pore regulation by reticular chemistry is an effective approach to develop MOFs with optimal pore structures for molecular separation. Further computational calculation and modelling confirmed that the pore window plays an important role in the molecular sieving of alkane isomers. Interestingly, $abtc^{4-}$ and $tptc^{4-}$, which are analogous to $bptc^{4-}$ but with increasing aspect ratio, did not lead into **ftw**-structures when combined with Zr–oxo clusters. Instead, they form **scu** and **lvt** topology built on 8- and 4-connected Zr_6 SBUs, respectively. This indicates that, while in previously reported **ftw**-MOFs rectangular ligands can fit into the structure by alternating their orientations and rotating the 12-connected inorganic SBU, there is a limited range of aspect ratios for a tetratopic ligand to be accommodated into an **ftw** structure. That is, when the geometry of an organic linker deviates too much from a square, it may not match the symmetry requirement for an **ftw** net or the targeted structure is not thermodynamically favoured. This would lead to the formation of an **ftw** derivative with reduced SBU connectivity.

Based on the above observations, in a follow-up study the same research group explored **ftw**-Y-MOFs with the same series of ligands.[29] As demonstrated by Eddaoudi

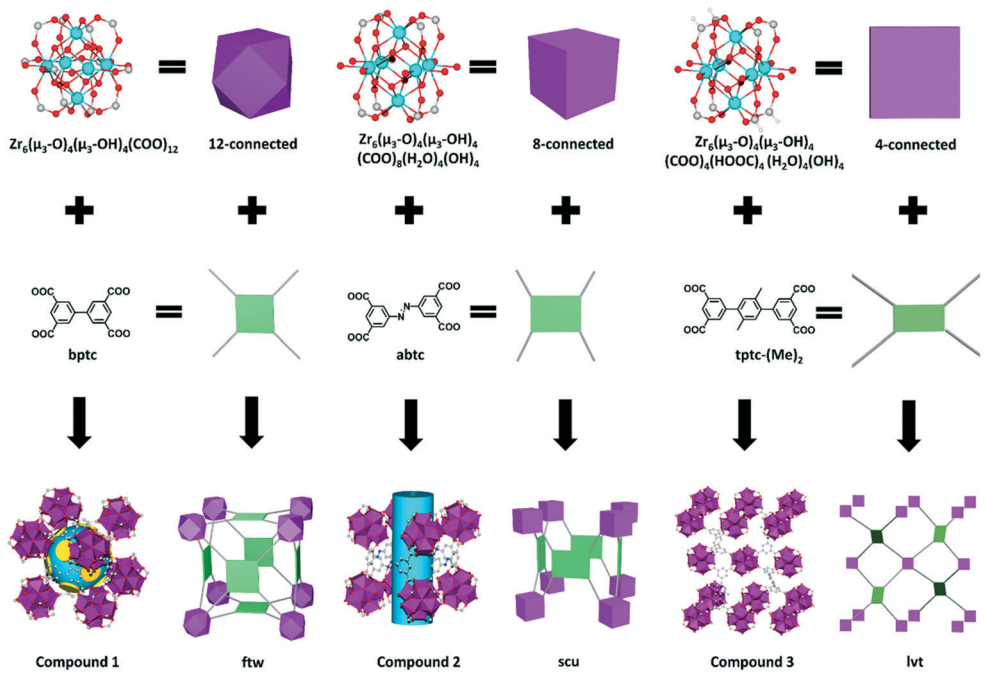

Fig. 5 Topology-directed design of **ftw**-Zr-bptc and its derivative structures with **scu** and **lvt** topology. Reproduced with permission.[18] Copyright 2018, springer nature.

et al., hexanuclear Y_6 (or many other rare earth metals) clusters behave similarly to Zr_6. They feature the same connectivity and can both fit into **ftw** or other related topology. For example, Y-bptc features the same connectivity and topology as that of Zr-bptc. The authors in this work also demonstrated that **ftw**-Y-MOFs have a higher tolerance with regard to the aspect ratio of the organic ligands. With the incorporation of $abtc^{4-}$, **ftw**-type Y-abtc was formed while the Zr-analogue adopts an **scu** structure. In addition, as a result of the different valence of Y^{3+} and Zr^{4+}, **ftw**-Y-MOFs form anionic frameworks with charge balancing cations dimethylammonium (DMA) residing inside the cages. Thus the DMA cations act as a new pore size regulator as a supplement to ligand dimensions. This allows the authors to fine-tune the pore size of **ftw**-MOFs with an added parameter. Indeed, the authors demonstrated that Y-abtc features optimal pore aperture for highly efficient separation of propane and propylene through selective molecular exclusion. It adsorbs 2.0 mmol g^{-1} of propylene but fully excludes propane under ambient conditions. The function of the DMA cations as a pore size regulator was further confirmed experimentally. When the material was activated at 200 °C without interfering with the DMA cations, a full separation of propane and propylene was achieved. However, when the activation temperature was increased to 300 °C, DMA cations underwent decomposition leaving protons as charge balancing cations. This led to the expansion of the effective pore size as reflected by the notably increased adsorption capacity of both propane and propylene. It is noteworthy that its Tb analogue Tb-abtc, reported by Eddaoudi and coworkers, also features the **ftw** topology and exhibits kinetic separation of propane and propylene.[30]

More recently, Yu *et al.* developed a new **ftw**-Y-MOF, HIAM-301, in this family which shows substantially improved separation efficiency for propane and propylene.[37] As a result of the relatively large aspect ratio of the organic linker $eddi^{4-}$, the formed **ftw**-network of HIAM-301 featured notable structure distortion and the cubic cage was twisted and deformed (Fig. 6). This was also observed in the aforementioned Y-abtc. HIAM-301 retained the molecular sieving behavior toward propane and propylene. It adsorbs propylene but full excludes propane under ambient conditions. Notably, its adsorption capacity for propylene is substantially higher than that of the other reported adsorbents showing selective molecular separation behavior, including KAUST-7, Co-gallate, Y-abtc, and JNU-7. Its propylene uptake at room temperature is 3.16 mmol g^{-1}. This should be attributed to its relatively large pore volume. The selective molecular exclusion behavior of HIAM-301 and host–guest interaction dynamics were confirmed and investigated by *in situ* neutron powder diffraction (NPD) and inelastic neutron scattering studies. NPD analysis confirmed that the DMA cations reside in the cage near the window and thus would regulate the pore aperture of the MOF. The preferential adsorption site for propylene was revealed to be between two adjacent Y_6 clusters where the adsorbed propylene was anchored through strong hydrogen bonds.

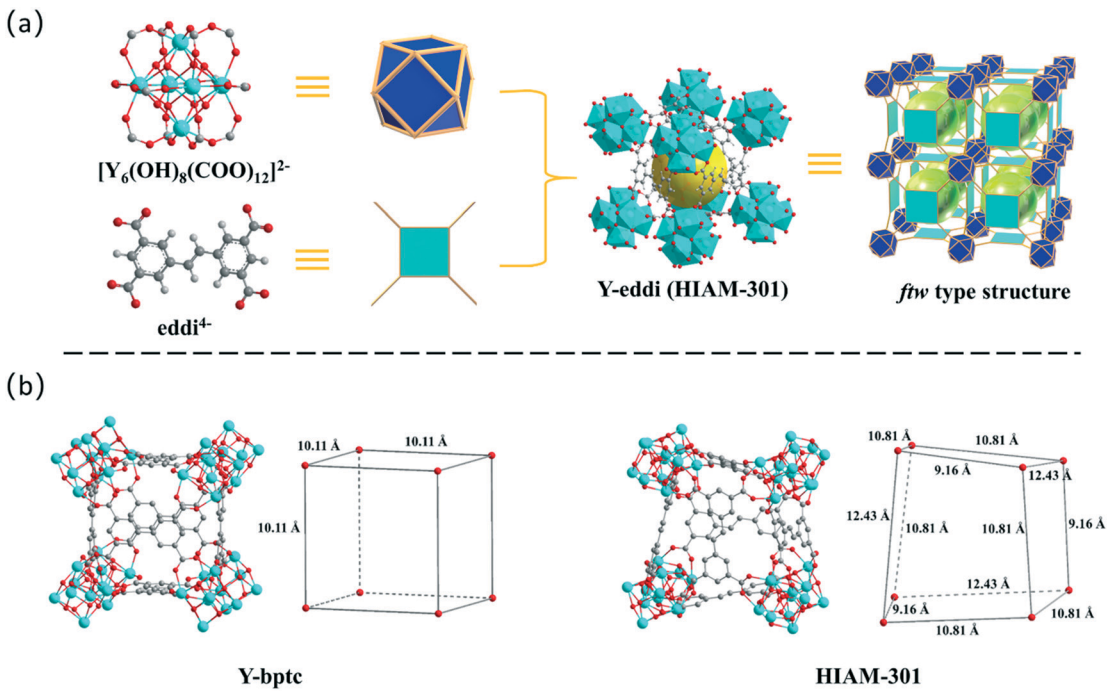

Fig. 6 (a) Inorganic and organic building units, crystal structure, and topology of HIAM-301. (b) Pore distortion of HIAM-301 compared to the perfect cubic cage of Y-bptc and the shape of the cage depicted by connecting eight equivalent μ3-O atoms from the vertexes. Reproduced with permission.[37] Copyright 2021, American Chemical Society.

5. Other novel **ftw**-MOFs

Besides the aforementioned early transition metals and rare earth metals (Zr, Hf, Y, Tb, Eu, *etc.*), late transition metals such as Ni^{2+} has also been employed for the construction of **ftw**-MOFs. Zhou *et al.* reported a series of **ftw**-MOFs built on a 12-connected $Ni_8(OH)_4(H_2O)_2(Pz)_{12}$ (Pz = pyrazolate) cluster and tetra-pyrazolate linkers.[14–16] The first reported member of this family is PCN-601 combining Ni_8 nodes and the porphrinic tetrapyrazolate ligand (H_4TPP).[16] The connecting mode of the Ni_8 node is similar to that of the commonly observed 12-connected Zr_6 cluster, which is propagated through Ni–pyrazolate rather than the Zr–carboxylate connection (Fig. 7). This different coordination connection leads to the excellent chemical stability of PCN-601 in alkali solutions which is not common for MOFs particularly those built on carboxylate linkers. PCN-601 retained its crystallinity and porosity in saturated sodium hydroxide solution at room temperature and 100 °C. The development of PCN-601 opens a door to a new family of base-resistant MOFs that may broaden their potential applications. The BET surface of PCN-601 is 1309 $m^2\ g^{-1}$. However, as a result of the relatively small organic ligand, its window size is too small to accommodate some reactant molecules. Thus the active sites of PCN-601 may not be accessible for certain substrates important for catalytic applications.

To address this issue, in the follow-up study the authors augmented the pore window of the MOF through isoreticular expansion.[15] The ligand was substituted by an elongated linker $TPPP^{4-}$ with one additional benzene ring added on each arm of the original TPP^{4-} and a new MOF, PCN-602, was achieved with **ftw**-topology. Indeed, as a result of the use of the elongated ligand, PCN-602 showed a BET surface area of 2219 $m^2\ g^{-1}$ and a window size of 6.3 × 14.2 Å. The pore dimension is notably larger than that of its parent structure PCN-601 which is 2.1 × 8.0 Å. Importantly, PCN-602 retained the exceptional chemical stability in hydroxide solution. It exhibited high catalytic activity for the C–H bond halogenation reaction in a basic system, outperforming the homogeneous counterpart. In a more recent study, the same research group further tailored the MOF by fluoro-functionalization of the benzene ring of TPP^{4-} and generated a new analogue, PCN-624.[14] As expected, the topology-directed modification didn't affect its chemical stability. In addition, the perfluorophenylene group decorated pore surface exhibited selective capture of guest molecules. And it showed high catalytic activity for the selective synthesis of fullerene–anthracene bisaddut.

The **ftw**-MOFs discussed above are generally constructed on a hexanuclear SBU and a tetratopic organic ligand. There are also reports of **ftw**-MOFs built on supermolecular building units. That is, their 12-connected nodes and/or 4-connected struts are coordinating complexes rather than an individual metal–oxo cluster or an organic ligand. Early in 2011, Bu *et al.* reported a microporous MOF featuring **ftw**-like structure based on supermolecular building blocks.[19] The overall structure can be topologically viewed as either a (3,4,4)-connected ternary net or a (4,12)-connected binodal net. For the latter, both 12-c vertexes and 4-c struts are actually multinuclear Co-based supermolecular coordination building blocks. This could be the underlying reason why the structure is not as stable as the common **ftw**-MOFs built on hexanuclear high valence metal clusters. Wade *et al.* reported the incorporation of a tetracarboxylate based palladium pincer complex into an **ftw**-Zr-MOF and its improved catalytic activity and stability upon immobilization.[28] Rosi *et al.* reported a series of heterobimetallic MOFs with different metal ions and clusters distributed throughout two or three inorganic SBUs and achieved topologies including **ftw**.[17] Specifically, the authors used the bifunctional isonicotinate linker with Co^{2+} to form a

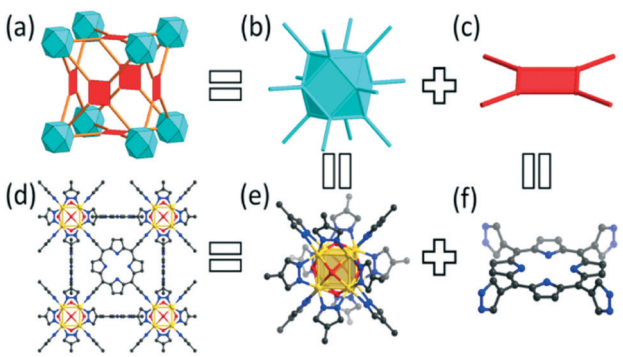

Fig. 7 Structural analysis of PCN-601. (a) **ftw**-a topology; (b) O_h symmetric 12-connected node; (c) D_{4h} symmetric 4-connected node; (d) PCN-601 (Ni atoms in the porphyrin center are omitted for clarity); (e) [Ni_8] cluster moiety; (f) TPP4– ligand. Reproduced with permission.[16] Copyright 2016, American Chemical Society.

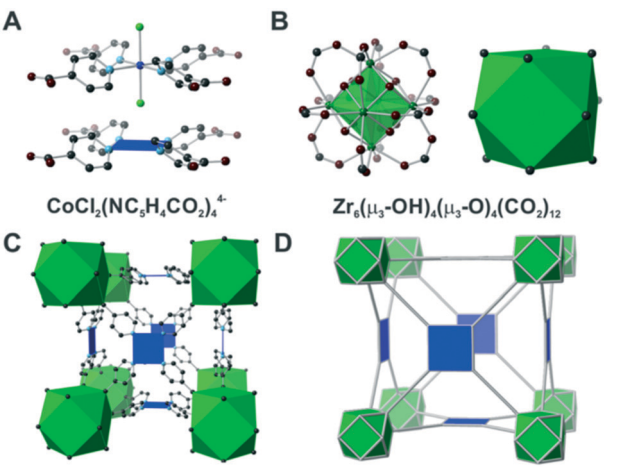

Fig. 8 MOF-1211 structure. (A) Square planar $CoCl_2(NC_5H_4CO_2^-)_4$ SBB (Co^{2+}, dark blue; N, light blue; Cl, light green; C, dark gray; O, red; $CoCl_2N_4$, blue squares; H atoms omitted; $NC_5H_4CO_2^-$ ligands are 2-fold rotationally disordered, and only one position is shown). (B) Zr SBU. Left: $Zr_6(\mu_3\text{-}O)_4(\mu_3\text{-}OH)_4(CO_2)_{12}$ cluster (Zr^{4+}, dark green) in which the green octahedron defines the Zr_6 core. Right: polyhedral representation of SBU. (C) MOF-1211(Zr/Co)crystal structure. (D) **ftw**-a net. Reproduced with permission.[17] Copyright 2018, American Chemical Society.

tetracarboxylate based square building unit through the coordination between Co^{2+} and the pyridyl groups (Fig. 8). And further combination of the tetracarboxyates and hexanuclear Zr_6 clusters form an **ftw**-type structure. The design strategy for heterobimetallic MOFs with targeted topology described in this work may be applicable to develop other MOFs. Similarly in a more recent work, Maspoch *et al.* reported a series of MOFs built on polycarboxylate rhodium metal–organic polyhedra (MOPs).[35] By employing isonicotinate or 1,3,5-benzenetricarboxylate, rhodium-based 12-connected cuboctahedral or 24-connected rhombicuboctahedral MOP supermolecular building blocks (MBBs) can be formed. The combination of these MBBs and other metal centers would form MOFs with different topologies. For example, the 12-connected cuboctahedral MBB can be connected through another 4-connected Cu_2 paddle-wheel units to form a (4,12)-connected **ftw**-MOF. The design strategy is potentially useful for developing MOFs with different functionalities with **ftw** and other topologies.

Conclusions

We have, in this highlight article, reviewed the progress in developing MOFs with **ftw** topology, with an emphasis on the implementation of reticular chemistry for achieving tailored structures with targeted properties. **ftw**-MOFs represent an important subgroup of MOFs. They have been extensively studied and hold enormous promise for certain applications such as separation of gases and vapors. As illustrated above, the 12-connected nodes in an **ftw** structure could be hexanuclear metal clusters including Zr_6, Hf_6, Y_6, Ln_6, *etc.*, or octanuclear metal clusters such as Ni_8, and the 4-connected struts could be tetracarboxylate or tetrapyrazolate based organic linkers. In addition, both the nodes and the struts could also coordinate supermolecular building blocks. As a result of the rotation of the 12-connected cuboctahedral nodes and the alternation of organic linkers, rectangular ligands with slight deviation from a square shape can also fit into the **ftw** structure. This has largely enriched the **ftw**-MOF family and contributed to their structural diversity.

MOFs with **ftw** topology generally feature highly robust structure and high porosity. However, previous studies focus more on their structures while numerous potential applications have not been extensively explored. This could be a future direction. Considering their high stability, porosity, and tunability, **ftw**-MOFs hold great promise for applications such as gas storage, catalysis, *etc.* In addition, when the pore size of **ftw**-MOFs falls to the ultramicroporous region, they are potentially suitable for gas/vapor separation. One possible challenge could be that the availability of tetratopic organic linkers may limit the fine-tuning of their pore apertures for highly efficient separation of small gases. To this end, the above-mentioned design strategies of employing supermolecular building blocks and introducing small charge balancing cations may be effective in addressing such a challenge.

Author contributions

X. L., H. W., and J. L. wrote the paper and all authors contributed to the discussion and final proof of the manuscript.

Conflicts of interest

There are no conflicts to declare.

Acknowledgements

We thank the Guangdong Natural Science Foundation (2019A1515010692) and Shenzhen Science and Technology Program (No. JCYJ20190809145615620, RCYX20200714114539243).

Notes and references

1 H. Furukawa, E. Cordova Kyle, M. O'Keeffe and M. Yaghi Omar, *Science*, 2013, **341**, 1230444.
2 M. Eddaoudi, J. Kim, N. Rosi, D. Vodak, J. Wachter, M. O'Keeffe and M. Yaghi Omar, *Science*, 2002, **295**, 469–472.
3 H. Deng, S. Grunder, E. Cordova Kyle, C. Valente, H. Furukawa, M. Hmadeh, F. Gándara, C. Whalley Adam, Z. Liu, S. Asahina, H. Kazumori, M. O'Keeffe, O. Terasaki, J. F. Stoddart and M. Yaghi Omar, *Science*, 2012, **336**, 1018–1023.
4 J. H. Cavka, S. Jakobsen, U. Olsbye, N. Guillou, C. Lamberti, S. Bordiga and K. P. Lillerud, *J. Am. Chem. Soc.*, 2008, **130**, 13850–13851.
5 Y. Bai, Y. Dou, L.-H. Xie, W. Rutledge, J.-R. Li and H.-C. Zhou, *Chem. Soc. Rev.*, 2016, **45**, 2327–2367.
6 Z. Hu and D. Zhao, *Dalton Trans.*, 2015, **44**, 19018–19040.
7 K.-K. Yee, N. Reimer, J. Liu, S.-Y. Cheng, S.-M. Yiu, J. Weber, N. Stock and Z. Xu, *J. Am. Chem. Soc.*, 2013, **135**, 7795–7798.
8 H. Furukawa, F. Gándara, Y.-B. Zhang, J. Jiang, W. L. Queen, M. R. Hudson and O. M. Yaghi, *J. Am. Chem. Soc.*, 2014, **136**, 4369–4381.
9 P. Ji, T. Drake, A. Murakami, P. Oliveres, J. H. Skone and W. Lin, *J. Am. Chem. Soc.*, 2018, **140**, 10553–10561.
10 B. An, L. Zeng, M. Jia, Z. Li, Z. Lin, Y. Song, Y. Zhou, J. Cheng, C. Wang and W. Lin, *J. Am. Chem. Soc.*, 2017, **139**, 17747–17750.
11 X. Meng, B. Gui, D. Yuan, M. Zeller and C. Wang, *Sci. Adv.*, 2016, **2**, e160048.
12 J. Zheng, M. Wu, F. Jiang, W. Su and M. Hong, *Chem. Sci.*, 2015, **6**, 3466–3470.
13 R. Luebke, Y. Belmabkhout, Ł. J. Weseliński, A. J. Cairns, M. Alkordi, G. Norton, Ł. Wojtas, K. Adil and M. Eddaoudi, *Chem. Sci.*, 2015, **6**, 4095–4102.
14 N. Huang, K. Wang, H. Drake, P. Cai, J. Pang, J. Li, S. Che, L. Huang, Q. Wang and H.-C. Zhou, *J. Am. Chem. Soc.*, 2018, **140**, 6383–6390.
15 X.-L. Lv, K. Wang, B. Wang, J. Su, X. Zou, Y. Xie, J.-R. Li and H.-C. Zhou, *J. Am. Chem. Soc.*, 2017, **139**, 211–217.

16 K. Wang, X.-L. Lv, D. Feng, J. Li, S. Chen, J. Sun, L. Song, Y. Xie, J.-R. Li and H.-C. Zhou, *J. Am. Chem. Soc.*, 2016, **138**, 914–919.
17 P. F. Muldoon, C. Liu, C. C. Miller, S. B. Koby, A. Gamble Jarvi, T.-Y. Luo, S. Saxena, M. O'Keeffe and N. L. Rosi, *J. Am. Chem. Soc.*, 2018, **140**, 6194–6198.
18 H. Wang, X. Dong, J. Lin, S. J. Teat, S. Jensen, J. Cure, E. V. Alexandrov, Q. Xia, K. Tan, Q. Wang, D. H. Olson, D. M. Proserpio, Y. J. Chabal, T. Thonhauser, J. Sun, Y. Han and J. Li, *Nat. Commun.*, 2018, **9**, 1745.
19 Z. Chang, D.-S. Zhang, T.-L. Hu and X.-H. Bu, *Cryst. Growth Des.*, 2011, **11**, 2050–2053.
20 W. Morris, B. Volosskiy, S. Demir, F. Gándara, P. L. McGrier, H. Furukawa, D. Cascio, J. F. Stoddart and O. M. Yaghi, *Inorg. Chem.*, 2012, **51**, 6443–6445.
21 Z. Wei, Z.-Y. Gu, R. K. Arvapally, Y.-P. Chen, R. N. McDougald, J. F. Ivy, A. A. Yakovenko, D. Feng, M. A. Omary and H.-C. Zhou, *J. Am. Chem. Soc.*, 2014, **136**, 8269–8276.
22 O. V. Gutov, W. Bury, D. A. Gomez-Gualdron, V. Krungleviciute, D. Fairen-Jimenez, J. E. Mondloch, A. A. Sarjeant, S. S. Al-Juaid, R. Q. Snurr, J. T. Hupp, T. Yildirim and O. K. Farha, *Chem. – Eur. J.*, 2014, **20**, 12389–12393.
23 T.-F. Liu, D. Feng, Y.-P. Chen, L. Zou, M. Bosch, S. Yuan, Z. Wei, S. Fordham, K. Wang and H.-C. Zhou, *J. Am. Chem. Soc.*, 2015, **137**, 413–419.
24 T. C. Wang, W. Bury, D. A. Gómez-Gualdrón, N. A. Vermeulen, J. E. Mondloch, P. Deria, K. Zhang, P. Z. Moghadam, A. A. Sarjeant, R. Q. Snurr, J. F. Stoddart, J. T. Hupp and O. K. Farha, *J. Am. Chem. Soc.*, 2015, **137**, 3585–3591.
25 Q. Lin, X. Bu, A. Kong, C. Mao, X. Zhao, F. Bu and P. Feng, *J. Am. Chem. Soc.*, 2015, **137**, 2235–2238.
26 P. Deria, D. A. Gómez-Gualdrón, W. Bury, H. T. Schaef, T. C. Wang, P. K. Thallapally, A. A. Sarjeant, R. Q. Snurr, J. T. Hupp and O. K. Farha, *J. Am. Chem. Soc.*, 2015, **137**, 13183–13190.
27 S. B. Kalidindi, S. Nayak, M. E. Briggs, S. Jansat, A. P. Katsoulidis, G. J. Miller, J. E. Warren, D. Antypov, F. Corà, B. Slater, M. R. Prestly, C. Martí-Gastaldo and M. J. Rosseinsky, *Angew. Chem., Int. Ed.*, 2015, **54**, 221–226.
28 S. A. Burgess, A. Kassie, S. A. Baranowski, K. J. Fritzsching, K. Schmidt-Rohr, C. M. Brown and C. R. Wade, *J. Am. Chem. Soc.*, 2016, **138**, 1780–1783.
29 H. Wang, X. Dong, V. Colombo, Q. Wang, Y. Liu, W. Liu, X.-L. Wang, X.-Y. Huang, D. M. Proserpio, A. Sironi, Y. Han and J. Li, *Adv. Mater.*, 2018, **30**, 1805088.
30 D.-X. Xue, A. Cadiau, Ł. J. Weseliński, H. Jiang, P. M. Bhatt, A. Shkurenko, L. Wojtas, C. Zhijie, Y. Belmabkhout, K. Adil and M. Eddaoudi, *Chem. Commun.*, 2018, **54**, 6404–6407.
31 S. Gao, L. Zhao, P. Zhao, Y. Huang and H. Zhao, *Inorg. Chim. Acta*, 2018, **480**, 173–176.
32 X. Xu, S. Li, Q. Liu, Z. Liu, W. Yan, L. Zhao, W. Zhang, L. Zhang, F. Deng, H. Cong and H. Deng, *ACS Appl. Mater. Interfaces*, 2019, **11**, 973–981.
33 F. Hu, Z. Di, M. Wu, M. Hong and J. Li, *Cryst. Growth Des.*, 2019, **19**, 6381–6387.
34 Z. Duan, Y. Li, X. Xiao, X. Huang, X. Li, Y. Li, C. Zhang, H. Zhang, L. Li, Z. Lin, Y. Zhao and W. Huang, *ACS Appl. Mater. Interfaces*, 2020, **12**, 18715–18722.
35 T. Grancha, A. Carné-Sánchez, F. Zarekarizi, L. Hernández-López, J. Albalad, A. Khobotov, V. Guillerm, A. Morsali, J. Juanhuix, F. Gándara, I. Imaz and D. Maspoch, *Angew. Chem., Int. Ed.*, 2021, **60**, 5729–5733.
36 Y. Wang, C. Hao, W. Fan, M. Fu, X. Wang, Z. Wang, L. Zhu, Y. Li, X. Lu, F. Dai, Z. Kang, R. Wang, W. Guo, S. Hu and D. Sun, *Angew. Chem., Int. Ed.*, 2021, **60**, 11350–11358.
37 L. Yu, X. Han, H. Wang, S. Ullah, Q. Xia, W. Li, J. Li, I. da Silva, P. Manuel, S. Rudić, Y. Cheng, S. Yang, T. Thonhauser and J. Li, *J. Am. Chem. Soc.*, 2021, **143**, 19300–19305.
38 M. J. Katz, Z. J. Brown, Y. J. Colon, P. W. Siu, K. A. Scheidt, R. Q. Snurr, J. T. Hupp and O. K. Farha, *Chem. Commun.*, 2013, **49**, 9449–9451.

